GL-TR-89-0344
ENVIRONMENTAL RESEARCH PAPERS, NO. 1050

An Outline for the RTNEPH Infrared Atmospheric Water Vapor Attenuation Study

ROBERT PAUL d'ENTREMONT
JOHN-LUC MONCET
TODD R. MILLER
MICHAEL K. GRIFFIN
LARRY W. THOMASON
JAMES T. BUNTING
CRYSTAL BARKER SCHAAF

29 December 1989

ATMOSPHERIC SCIENCES DIVISION PROJECT 6670

GEOPHYSICS LABORATORY
HANSCOM AFB, MA 01731-5000

"This technical report has been reviewed and is approved for publication."

FOR THE COMMANDER,

KENNETH R. HARDY, Chief
Satellite Meteorology Branch

ROBERT A. McCLATCHEY, Director
Atmospheric Sciences Division

This document has been reviewed by the ESD Public Affairs Office (ESD/PA) and is releasable to the National Technical Information Service (NTIS).

Qualified requestors may obtain additional copies from the Defense Technical Information Center. All others should apply to the National Technical Information Service.

If your address has changed, or if you wish to be removed from the mailing list, or if the addressee is no longer employed by your organization, please notify AFGL/DAA, Hanscom AFB, MA 01731-5000. This will assist us in maintaining a current mailing list.

Do not return copies of this report unless contractual obligations or notices on a specific document require that it be returned.

REPORT DOCUMENTATION PAGE

Form Approved
OMB No. 0704-0188

1. AGENCY USE ONLY (Leave blank)	2. REPORT DATE	3. REPORT TYPE AND DATES COVERED
	29 December 1989	Scientific Interim

4. TITLE AND SUBTITLE
An Outline for the RTNEPH Infrared Atmospheric Water Vapor Attenuation Study

5. FUNDING NUMBERS
PE 62101F
PR 6670 TA 17 WU 07

6. AUTHOR(S)
Robert P. d'Entremont
Jean-Luc Moncet*
Todd R. Miller*
Michael K. Griffin
Larry W. Thomason
James T. Bunting
Crystal Barker Schaaf

7. PERFORMING ORGANIZATION NAME(S) AND ADDRESS(ES)
Geophysics Laboratory (LYS)
Hanscom AFB
Massachusetts 01731-5000

8. PERFORMING ORGANIZATION REPORT NUMBER
GL-TR-89-0344
ERP, No. 1050

9. SPONSORING / MONITORING AGENCY NAME(S) AND ADDRESS(ES)

10. SPONSORING / MONITORING AGENCY REPORT NUMBER

11. SUPPLEMENTARY NOTES
* Atmospheric & Environmental Research Inc, 840 Memorial Drive, Cambridge, MA 02139

12a. DISTRIBUTION / AVAILABILITY STATEMENT
Approved for public release; distribution unlimited

12b. DISTRIBUTION CODE

13. ABSTRACT *(Maximum 200 words)*

The Real-Time Nephanalysis (RTNEPH) generates real-time global analysis of cloud extent, base, height, and type. The RTNEPH makes extensive use of satellite data that are measured in the 10-12 μm infrared (IR) window for thermal mapping of clouds and the earth's surface both day and night. Water vapor absorption effects are significant in such data, especially for high viewing angles and tropical atmospheres where water vapor concentrations are generally high. Water vapor attenuates the emitted ground radiance, reducing its magnitude and with it the apparent temperature of the surface being viewed. Currently, the RTNEPH takes into account such attenuation losses using lookup tables that are functions of viewing geometry, time of day, type of background, and the like. However, these corrections have limited value and leave room for significant improvement. This report outlines and presents two new techniques that are expected to enhance the attenuation correction capabilities of the RTNEPH, multivariate polynomial regression (the Weinreb technique) and the correlated K method.

14. SUBJECT TERMS
Transmittance
Water vapor attenuation
Infrared
Cloud analysis

15. NUMBER OF PAGES
50

16. PRICE CODE

17. SECURITY CLASSIFICATION OF REPORT	18. SECURITY CLASSIFICATION OF THIS PAGE	19. SECURITY CLASSIFICATION OF ABSTRACT	20. LIMITATION OF ABSTRACT
UNCLASSIFIED	UNCLASSIFIED	UNCLASSIFIED	SAR

Preface

The authors wish to express their gratitude to Barbara A. Main for her help in preparing the figures that appear in this report, and to Joan Ward and Jean I. F. King for their thoughtful suggestions and assistance in proofreading the text. Thanks are also extended to Capt Thomas Hamill and Capt James Cramer of AFGWC for their many helpful discussions.

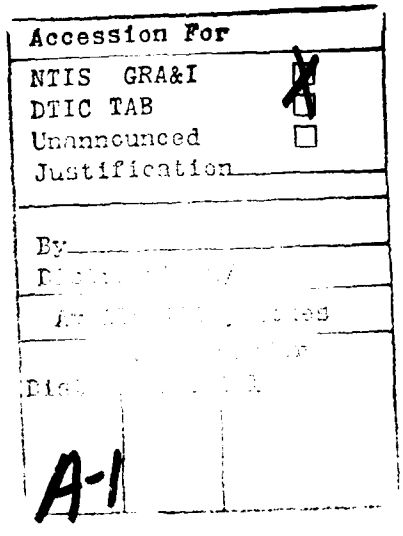

Contents

Illustrations

An Outline for the RTNEPH Infrared Atmospheric Water Vapor Attenuation Study

1. BACKGROUND

Real-Time Nephanalysis (RTNEPH) is an automated cloud analysis model that is in operational use at the Air Force Global Weather Central (AFGWC). In the RTNEPH, polar-orbiting-satellite imagery is analyzed in conjunction with conventional meteorological cloud observations to produce a global analysis of cloud attributes such as extent, height, bases, and type. The RTNEPH and its predecessor, the Three-Dimensional Nephanalysis (3DNEPH), have been generating real-time global cloud analyses since 1970 (see Fye, 1978; Kiess and Cox, 1988). RTNEPH cloud analyses are used primarily to initialize cloud forecast models in support of Air Force missions; they are also archived for use by the research community as one of the few sources of long-term global cloud climatologies available today.

RTNEPH makes extensive use of satellite data measured in the 10-12μm infrared (IR) window for the thermal mapping of clouds and the earth's surface both day and night. Although at first approximation this part of the spectrum is generally considered free of water vapor absorption effects, attenuation is significant for high viewing angles and tropical atmospheres. Thermal radiation emitted by the ground is attenuated, primarily by water vapor, as it travels up through a cloud-free atmosphere. The net effect is that the radiance observed by the satellite is less than the radiance emitted by the underlying surface, causing that surface to appear colder than it truly is.

The RTNEPH uses a threshold technique whereby a satellite-measured IR brightness temperature is compared to the actual skin temperature of the surface

Received for Publication 20 December 1989

being observed. If the brightness temperature is equal to the true ground temperature, the scene is considered cloud free; if it is lower, the scene is determined to contain cloud. The underlying assumptions are that: 1) temperature generally decreases with height throughout the troposphere, and 2) clouds are always physically colder than the ground; therefore their temperatures are always lower than the ground temperature. (Obviously the presence of low-level temperature inversions invalidates this assumption. How to handle inversions is an issue (aside from attenuation) that needs to be addressed more carefully in the RTNEPH.)

Water vapor attenuates the emitted ground radiance, reducing its magnitude and with it the apparent temperature of the surface being viewed. Without an attenuation correction being applied to the satellite brightness temperature measurement, it will almost always be lower than the skin temperature of the surface being viewed. If a raw satellite-measured brightness temperature is compared directly with the actual surface skin temperature, the RTNEPH will always flag a scene as containing clouds. Thus it is easy to see the importance of properly accounting for attenuation losses in IR brightness temperature measurements before they are processed by cloud detection algorithms.

In recent years the Geophysics Laboratory has been actively involved in proposing and developing improvements for the RTNEPH (Bunting et al., 1983; d'Entremont et al., 1982; d'Entremont et al., 1989). It is the intent of this report to outline in detail a new study designed to enhance the cloud detection capability of the RTNEPH by more effectively handling the effects that atmospheric water vapor attenuation have on satellite brightness temperature measurements at IR wavelengths; upon completion, results of this study will be published in a subsequent paper. First, atmospheric water vapor attenuation theory will be presented in Sections 2 and 3, followed by a discussion in Sections 4-7 on how to apply this theory to the RTNEPH in as accurate and sensible a manner as possible. Section 8 outlines the plans for developing and incorporating a water vapor attenuation model into the RTNEPH, taking into consideration both the type and accuracy of the atmospheric data that the RTNEPH has (or soon will have) available for use.

2. NOTATION

I_λ	Monochromatic Upwelling Thermal Radiance, $W\ m^{-2}\ \mu m^{-1}\ ster^{-1}$ [$M\ L^{-1}\ T^{-3}$]
$B_\lambda(T)$	Monochromatic Planck Blackbody Radiance, $W\ m^{-2}\ \mu m^{-1}\ ster^{-1}$ [$M\ L^{-1}\ T^{-3}$]
λ	Wavelength, μm [L]
T	Temperature, K [θ]
$\tau_\lambda(p)$	Atmospheric Transmittance, Dimensionless
ϵ_λ	Monochromatic Emissivity, Dimensionless
r_λ	Monochromatic Reflectivity, Dimensionless
t_λ	Monochromatic Transmissivity, Dimensionless
I_j	Average Spectral Upwelling Thermal Radiance, $W\ m^{-2}\ \mu m^{-1}\ ster^{-1}$ [$M\ L^{-1}\ T^{-3}$]
$\phi_j(\lambda)$	Sensor Response Function for Satellite Sensor *j*, Dimensionless

3. RADIATIVE TRANSFER THEORY

The monochromatic upwelling thermal radiance at the top of a non-scattering, plane-parallel, cloud free atmosphere that is in local thermodynamic equilibrium and whose source function is the Planck function may be written in the form

$$I_\lambda = \epsilon_{\lambda,sfc} B_\lambda(T_{sfc}) \tau_{\lambda,sfc} + \int_{p_{sfc}}^{0} B_\lambda[T(p')] \frac{\partial \tau_\lambda}{\partial p'} dp' + r_{\lambda,sfc} \tau_{\lambda,sfc} \int_{0}^{p_{sfc}} B_\lambda[T(p')] \frac{\partial \tau'_\lambda}{\partial p'} dp', \quad (1)$$

where $\epsilon_{\lambda,sfc}$ is the emissivity of the earth's surface; $B_\lambda(T)$ is the Planck radiance emitted by a blackbody of temperature T at wavelength λ; $\tau_{\lambda,sfc}$ is the atmospheric transmittance at wavelength λ between the top of the atmosphere and the surface;

$\tau_\lambda \equiv \tau_\lambda(p)$ is the atmospheric transmittance at wavelength λ for the vertical path between the top of the atmosphere (at p=0) and any pressure level p in the atmosphere; $r_{\lambda,sfc}$ is the surface reflectivity ($r_{\lambda,sfc} = 1-\epsilon_{\lambda,sfc}$); and $\tau'_\lambda(p)$ is the transmittance between the surface at $p=p_{sfc}$ and any pressure level in the atmosphere p (note that $\tau_\lambda(p_{sfc}) = \tau'_\lambda(0) = \tau_{\lambda,sfc}$). The first term on the right side of Eq. (1) denotes the ground contribution to I_λ and is the dominant term in long-wavelength IR (LWIR) thermal window regions. The second term denotes the upwelling atmospheric emission, and the third term denotes the atmospheric emission radiated in the downward direction and reflected back up by the surface.

The Planck blackbody emission $B_\Lambda(T)$ for a blackbody of temperature T, wavelength Λ, is given by

$$B_\Lambda(T) = \frac{2hc^2\Lambda^{-5}}{e^{hc/K\Lambda T} - 1},$$

where Λ is in meters, T is in Kelvin, the Planck constant $h = 6.6262 \times 10^{-34}$ J sec, the speed of light $c = 2.998 \times 10^8$ m sec^{-1}, and Boltzmann's constant $K = 1.3806 \times 10^{-23}$ J K^{-1}. For convenience it can be rewritten in the form

$$B_\lambda(T) = \frac{c_1\lambda^{-5}}{e^{c_2/\lambda T} - 1}, \tag{2}$$

where $c_1 = 1.19107 \times 10^8$ W μm^4 m^{-2} ster^{-1}, $c_2 = 1.43883 \times 10^4$ μm K, T is in K, and where λ is now expressed in μm (instead of m). Using Eq. (2), the Planck radiance units are W m^{-2} μm^{-1} ster^{-1}.

Spaceborne satellite sensors are not designed to measure monochromatic radiances but radiant energies over some wavelength range $\lambda_1 \leq \lambda \leq \lambda_2$. The observed radiance I_j sensed by a downward-pointing radiometer in spectral band "j" is given by

$$I_j = \frac{\int_{\lambda_{j1}}^{\lambda_{j2}} I_\lambda \, \phi_j(\lambda) d\lambda}{\int_{\lambda_{j1}}^{\lambda_{j2}} \phi_j(\lambda) d\lambda}, \tag{3}$$

where $\phi_j(\lambda)$ is the spectral response function for sensor j, with the j subscript in I_j denoting a spectrally weighted average radiance. The response function $\phi_j(\lambda)$ is a measure of sensor j's instrument response to radiation at wavelength λ; if $\phi_j(\lambda) = 1$, the sensor detects 100 percent of the energy radiated at wavelength λ, whereas if $\phi_j(\lambda) = 0.25$, then the sensor detects only 25 percent of energy radiated at

wavelength λ. Within some wavelength range $\lambda_{j1} \leq \lambda \leq \lambda_{j2}$, the response function $\phi_j(\lambda)$ for sensor j is a rapidly varying function of wavelength; outside this range it is zero. Response functions are specific to each sensor and indicate instrument sensitivity characteristics. Response functions for the NOAA Advanced Very High Resolution Radiometer (AVHRR) thermal channels 4 and 5 and the DMSS Operational Linescan-Thermal (OLS-T) channel are shown in Figure 1.

4. APPLICATION TO THE RTNEPH

Equations (1) and (3) are useful for computing water vapor attenuation effects in LWIR satellite radiance measurements. To adapt Eq. (1) for operational RTNEPH use, the following approximations are made. First, LWIR emissivities ϵ_λ for the ground and most opaque clouds are assumed to be one. With $\epsilon_{\lambda,sfc} = 1$, then $r_{\lambda,sfc} = 1 - \epsilon_{\lambda,sfc} = 0$, and Eq. (1) reduces to

$$R_\lambda = B_\lambda(T_{sfc})\tau_{\lambda,sfc} + \int_{p_{sfc}}^{0} B_\lambda[T(p')]\frac{\partial \tau_\lambda}{\partial p'}dp'. \qquad (4a)$$

Equation (4a) gives the form for the monochromatic radiance emitted by a blackbody surface (in this case, the ground) of temperature T_{sfc}. Substituting R_λ into Eq. (3) for I_λ yields

$$R_j = \frac{\int_{\lambda_{j1}}^{\lambda_{j2}} R_\lambda \, \phi_j(\lambda)d\lambda}{\int_{\lambda_{j1}}^{\lambda_{j2}} \phi_j(\lambda)d\lambda}, \qquad (4b)$$

where R_j is the satellite-observed radiance emitted by a blackbody surface and travelling through a cloud free atmosphere.

4.1 Cloud/No-Cloud Decisions

The RTNEPH has access to surface and upper air data that allow for the calculation of the expected satellite radiance as given by Eq. (4b). Surface skin temperatures T_{sfc} are available to the RTNEPH on an eighth-mesh (47 km) horizontal grid resolution. Thus, using Eq. (2), the Planck radiance term $B_\lambda(T_{sfc})$ on the right side of Eq. (4a) can be computed on an eighth-mesh basis. The temperature profile T(p) is available on a whole-mesh (376 km) resolution, allowing the atmospheric radiances $B_\lambda[T(p)]$ to be computed on a whole-mesh basis.

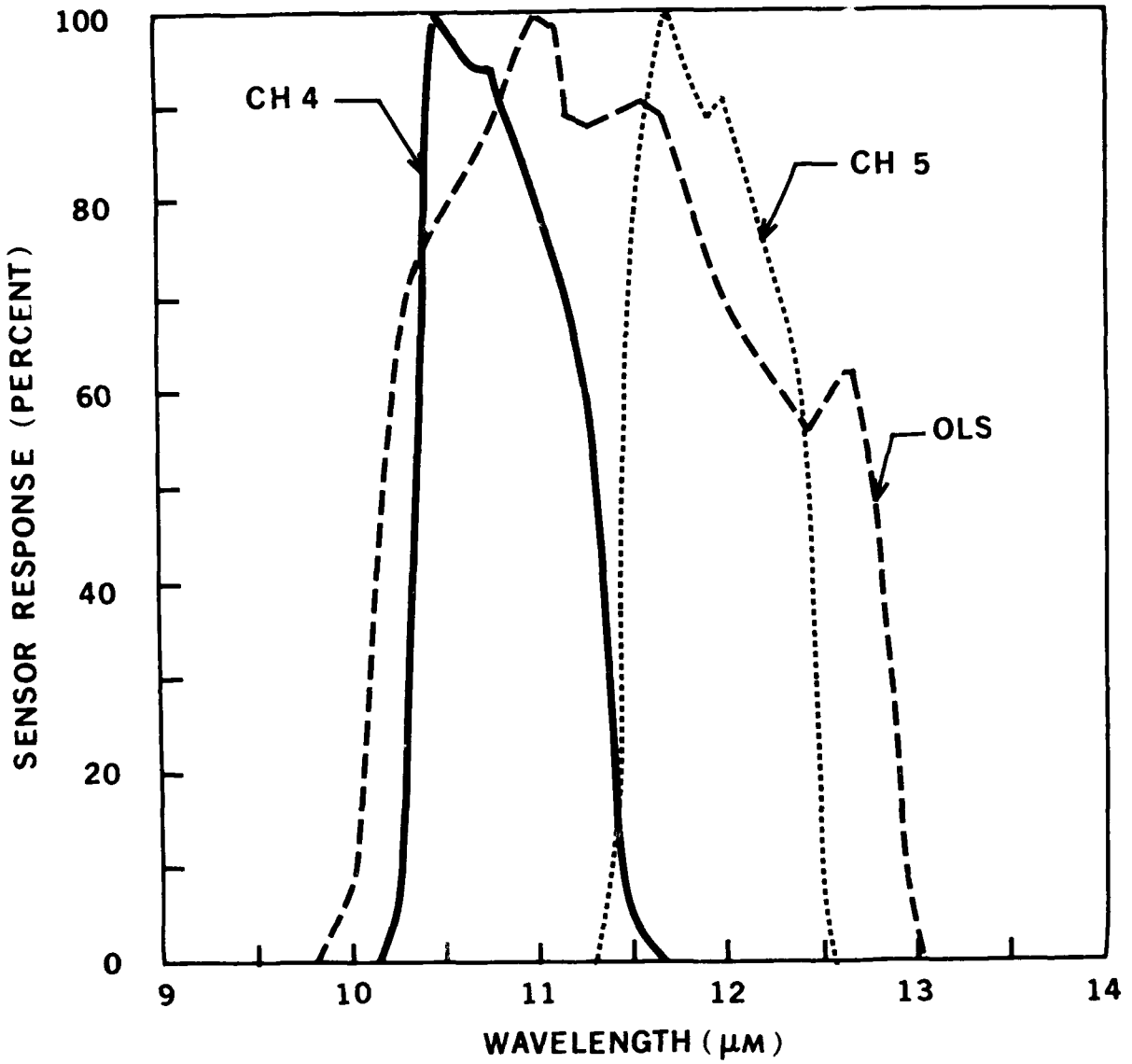

Figure 1. Response Functions for the NOAA AVHRR 10.7 and 11.8μm LWIR Channels 4 and 5, and the DMSS OLS-T Thermal Channel

The transmittance profile $\tau_\lambda(p)$ denotes the amount of atmospheric attenuation at wavelength λ between the top of the atmosphere and the level at pressure p. Transmittances can also be computed at whole-mesh resolution since, in the LWIR, τ_λ is (essentially) a function of temperature and water vapor profiles. The details of how the RTNEPH can compute transmittances in real-time are left for the next section; assume for now that the $\tau_\lambda(p)$ are provided at the whole-mesh resolution of the upper air profiles.

With surface skin temperature and the corresponding upper air temperature and transmittance profiles, the monochromatic radiance R_λ, and in turn, the spectrally averaged radiance R_j can be computed for each eighth-mesh grid point of the RTNEPH. Assuming that the atmospheric temperatures T(p) decrease monotonically with pressure, there is no way for a satellite-measured radiance I_{sat} from a cloudy field of view to be higher than the clear-column R_j. Thus R_j can be compared directly to I_{sat}: if $I_{sat} < R_j$, the scene contains clouds; if $I_{sat} = R_j$, the scene is cloud free.

One problem with using this approach is that the RTNEPH uses satellite-measured brightness temperatures T_{sat} from the Satellite Global Data Base (SGDB) to perform the cloud/no-cloud decision, not radiances I_{sat}. Thus, the computed radiances R_j must first be converted to an equivalent brightness temperature T_j using a brightness-temperature-to-radiance lookup table that is constructed in the following way:

$$B_j(T) = \frac{\int_{\lambda_{j1}}^{\lambda_{j2}} B_\lambda(T)\, \phi_j(\lambda) d\lambda}{\int_{\lambda_{j1}}^{\lambda_{j2}} \phi_j(\lambda) d\lambda}, \tag{5a}$$

where $B_\lambda(T)$ is given by Eq. (2). Equation (5a) relates temperature T to radiance B_j for satellite sensor j. By constructing a table of values $B_j(T)$ for a range of terrestrially expected temperatures T (say 190 - 330 K), it is possible to map a computed (or measured) radiance to a unique brightness temperature T_j by substituting R_j for B_j in Eq. (5a). Let this relation be denoted

$$T_j = T(R_j), \tag{5b}$$

where T_j is the equivalent brightness temperature corresponding to radiance measurement R_j, as defined by Eq. (5a).

Consider a scene in which a satellite measures a particular brightness temperature T_{sat} . A decision can be made as follows concerning whether the scene

contains cloud. First, determine the clear-column brightness temperature T_j from Eq. (5b) using the theoretically computed clear-column radiance R_j from Eq. (4). Then use T_j to compute a brightness temperature difference

$$\Delta T_j = T_{sfc} - T_j , \tag{6}$$

where T_{sfc} is the surface skin temperature from the RTNEPH database. When ΔT_j is added to the observed temperature T_{sat}, the result is the true physical temperature T_{sfc} of the ground being viewed. A direct comparison can be made between the surface skin temperature T_{sfc} and T^*, where

$$T^* = T_{sat} + \Delta T_j. \tag{7}$$

If the scene is cloud free, then $T^*=T_{sfc}$. If clouds are present, then $T^*<T_{sfc}$ since the clouds are colder; they emit less radiation, thereby showing a lower temperature than the warmer ground below.

Note that the effects of LWIR atmospheric attenuation are brought into the cloud/no-cloud decision via the transmittances τ_λ in the monochromatic upwelling radiance Eq. (4a). Thus, assuming that the skin temperatures T_{sfc} are reliable, the critical issue here is to compute the $\tau_\lambda(p)$ profiles as accurately as possible. This issue is addressed in Section 5.

4.2 Improved Cloud Top Height Calculations

If a blackbody is placed at some pressure level p^* within the atmosphere, then R_λ [from Eq. (4a)] can be written as a function of p^* in the form

$$R_\lambda(p^*) = B_\lambda[T(p^*)]\tau_\lambda(p^*) + \int_{p^*}^{0} B_\lambda[T(p')]\frac{\partial \tau_\lambda}{\partial p'}dp', \tag{8a}$$

where $R_\lambda(p^*)$ is the monochromatic upwelling radiance observed at the top of a cloud-free atmosphere within which lies a blackbody at pressure level $p = p^*$ [which can be converted to an altitude $z = z^*$ via the pressure-height profile $p(z)$]. Substituting $R_\lambda(p^*)$ for R_λ in (4b) yields the expected upwelling radiance for spectral band j:

$$R_j(p^*) = \frac{\int_{\lambda_{j1}}^{\lambda_{j2}} R_\lambda(p^*)\,\phi_j(\lambda)d\lambda}{\int_{\lambda_{j1}}^{\lambda_{j2}} \phi_j(\lambda)d\lambda}, \tag{8b}$$

where $R_j(p^*)$ is the radiance emitted through a cloud free atmosphere by a blackbody at pressure level p^*, and measured by satellite sensor *j*. A profile of expected brightness temperatures $T_j(p^*)$ can be computed for different p^*'s using Eq. (8), where

$$T_j(p^*) = T[R_j(p^*)] \tag{8c}$$

from Eq. (5b).

Now consider the blackbody at pressure level p^* to be a cloud. Assuming (as the RTNEPH does) that the cloud completely fills the pixel field of view, a profile of ΔT_j's can be computed:

$$\Delta T_j(p) = T(p) - T_j(p), \tag{9}$$

where $T(p)$ is the atmospheric temperature at pressure level p, and $T_j(p)$ is given by Eq. (8c). $T_j(p)$ is the brightness temperature that the satellite would measure if the top of a blackbody cloud lies at pressure level p [which again can be converted to a cloud top altitude z via the p(z) profile].

Now assume that the RTNEPH has properly made a cloud decision for a pixel based on Eq. (7). Consider the cloud top to be at pressure level p. The measured brightness temperature T_{sat} for that cloudy pixel will be less than the true cloud temperature due to attenuation by the atmosphere above the cloud. The cloud top temperature T_{cld} is given by

$$T_{cld} = T_{sat} + \Delta T_j(p_{cld}), \tag{10}$$

where p_{cld} is the pressure level at the cloud top, and $\Delta T_j(p_{cld})$ is computed from Eq. (9) with $p = p_{cld}$. Note that Eq. (10) reduces to Eq. (7) for $p_{cld}=p_{sfc}$.

The true physical temperature T_{cld} for a cloud top at pressure level p_{cld} is given precisely by Eq. (10) for optically thick clouds [that is, for clouds whose emissivity is unity; see Eq. (4a)]. Equation (10) can be used operationally by the RTNEPH in adjusting cloud top temperatures to a more accurate value as long as the cloud top pressure is known. Obviously, the RTNEPH has no way of knowing *a priori* what p_{cld} is. However, a good estimate for p_{cld} can be found by matching an uncorrected, cloudy brightness temperature T_{sat} (from the SGDB) directly to a first-guess pressure p_{init} using the upper air temperature-height profile $T(p)$. Substituting p_{init} for p_{cld} in Eq. (10) yields

$$T_{cld} \approx T_{sat} + \Delta T_j(p_{init}).$$

In turn, this estimate for T_{cld} can be matched with an improved estimate of p_{cld}, again using the T(p) profile.

4.3 Improved Surface Skin Temperature Analysis

The computation of water vapor attenuation effects using radiative transfer theory has potential not only for cloud/no-cloud decisions and improved cloud top estimates, but for improving surface skin temperature measurements as well.

For notational simplicity, define the normalized response function $\phi_j^*(\lambda)$ to be

$$\phi_j^*(\lambda) = \frac{\phi_j(\lambda)}{\int_{\lambda_{j2}}^{\lambda_{j1}} \phi_j(\lambda)d\lambda}, \tag{11}$$

where $\phi_j(\lambda)$ is the response function for sensor j. Now consider the case when the RTNEPH confidently decides that a pixel of brightness temperature T_{sat} is cloud free. Using Eq. (11), the satellite radiance as given by Eq. (4b) is written

$$R_j = \int_{\lambda_{j1}}^{\lambda_{j2}} R_\lambda \, \phi_j^*(\lambda) \, d\lambda. \tag{12}$$

Substituting (4a) for R_λ into (12) yields

$$R_j = \int_{\lambda_{j1}}^{\lambda_{j2}} \phi_j^*(\lambda) \, B_\lambda(T_{sfc}) \, \tau_{\lambda,sfc} \, d\lambda + \int_{\lambda_{j1}}^{\lambda_{j2}} \phi_j^*(\lambda) \int_{p_{sfc}}^{0} B_\lambda[T(p')] \frac{\partial \tau_\lambda}{\partial p'} dp' \, d\lambda. \tag{13}$$

Expand $B_\lambda(T_{sfc})$ [in the first term on the right side of Eq. (13)] into a Taylor series about the measured satellite brightness temperature T_{sat} to obtain

$$B_\lambda(T_{sfc}) \approx B_\lambda(T_{sat}) + (T_{sfc} - T_{sat}) \frac{\partial B_\lambda(T_{sat})}{\partial T} + \cdots .$$

For $|T_{sfc} - T_{sat}| \leq \sim 15K$, terms of second order and higher can be neglected since their sum is small in comparison to the first-order term. Substituting the truncated Taylor expansion back into Eq. (13) yields

$$R_j = \int_{\lambda_{j1}}^{\lambda_{j2}} \phi_j^*(\lambda) \, B_\lambda(T_{sat}) \tau_{\lambda,sfc} d\lambda + (T_{sfc} - T_{sat}) \int_{\lambda_{j1}}^{\lambda_{j2}} \phi_j^*(\lambda) \, \tau_{\lambda,sfc} \frac{\partial B_\lambda(T_{sat})}{\partial T} \, d\lambda$$

$$+ \int_{\lambda_{j1}}^{\lambda_{j2}} \phi_j^*(\lambda) \int_{p_{sfc}}^{0} B_\lambda[T(p')] \frac{\partial \tau_\lambda}{\partial p'} dp' \, d\lambda.$$

Solving for T_{sfc} finally yields

$$T_{sfc} = \frac{R_j - \int_{\lambda_{j1}}^{\lambda_{j2}} \phi_j^*(\lambda) \left\{ B_\lambda(T_{sat})\tau_{\lambda,sfc} + \int_{p_{sfc}}^{0} B_\lambda[T(p')] \frac{\partial \tau_\lambda}{\partial p'} dp' \right\} d\lambda}{\int_{\lambda_{j1}}^{\lambda_{j2}} \phi_j^*(\lambda)\, \tau_{\lambda,sfc} \frac{\partial B_\lambda(T_{sat})}{\partial T} d\lambda} + T_{sat}\,, \tag{14}$$

where T_{sfc} is the desired surface skin temperature, and T_{sat} is the clear-column brightness temperature measurement. The $\partial B/\partial T$ term in the denominator of Eq. (14) is derived analytically by differentiating Eq. (2) with respect to temperature to obtain

$$\frac{\partial B_\lambda(T)}{\partial T} = \frac{1}{T^2} \frac{c_1 c_2 \lambda^{-6} e^{c_2/\lambda T}}{(e^{c_2/\lambda T} - 1)^2}, \tag{15}$$

and substituting T_{sat} for T. The constants c_1 and c_2 are as given for Eq. (2).

Equation (14) can be used in the RTNEPH to compute a surface skin temperature T_{sfc} whenever a clear-column brightness temperature T_{sat} is available along with coincident upper-air data sufficient to compute a transmittance profile $\tau_\lambda(p)$.

Another method for computing surface skin temperatures from clear-column brightness temperatures is also applicable to RTNEPH use. This method is perhaps more straightforward than Eq. (14) in obtaining a value for T_{sfc}, but may be somewhat more difficult to apply. Define the central wavelength for sensor j to be some λ_j that satisfies

$$R_{\lambda_j} = R_j \quad \text{for some } \lambda_{j1} \le \lambda_j \le \lambda_{j2}, \tag{16}$$

where R_{λ_j} is given by Eq. (4a) with $\lambda = \lambda_j$, R_j is given by Eq. (4b), and λ_{j1}, λ_{j2} are as defined for Eq. (3). The existence of a λ_j is assured by the Mean Value Theorem. The central wavelength varies with temperature. The temperature dependence is weak enough, however, to keep λ_j nearly constant over a typical LWIR sensor bandwidth and typical terrestrial temperatures.

Solving Eq. (4a) with $\lambda = \lambda_j$ for the surface emission B_{λ_j} yields

$$B_{\lambda_j}(T_{sfc}) = \frac{I_{sat} - \int_{p_{sfc}}^{0} B_{\lambda_j}[T(p)] \frac{\partial \tau_{\lambda_j}}{\partial p'} dp'}{\tau_{\lambda_j, sfc}}, \quad (17)$$

where I_{sat} is the measured clear-column radiance, replacing R_{λ_j} in Eq. (4a). Equation (17) can be used to calculate the surface emission whenever a cloud-free radiance measurement is available from satellite. If the satellite brightness temperature measurement is provided (as is the case for the RTNEPH SGDB data), then an I_{sat} can be computed using Eq. (2) with $T = T_{sat}$ and $\lambda = \lambda_j$.

Having computed $B_{\lambda_j}(T_{sfc})$, it can then be converted to surface skin temperature T_{sfc} in the following way. Solving Eq. (2) for T yields

$$T = \frac{c_2}{\lambda} \frac{1}{\ln\left[\frac{c_1}{\lambda^5 B_\lambda} + 1\right]},$$

which relates temperature T directly to radiance B_λ. If B_λ is replaced with $B_{\lambda_j}(T_{sfc})$, then the surface skin temperature T_{sfc} is simply

$$T_{sfc} = \frac{c_2}{\lambda_j} \frac{1}{\ln\left[\frac{c_1}{\lambda_j^5 B_{\lambda_j}} + 1\right]}, \quad (18)$$

where λ_j is the central wavelength, and B_{λ_j} is computed using Eq. (17) for a cloud-free atmosphere.

The success of Eq. (18) in computing T_{sfc} is sensitive to a proper choice of the central wavenumber λ_j, which varies as a function of both the surface skin temperature T_{sfc} and the temperature profile T(p). However, since atmospheric absorption is low, the dependence of λ_j on T_{sfc} is likely to be stronger than that on T(p). Fortunately for LWIR regions, the Planck radiance varies slowly with temperature, so that it is likely the central wavelength varies slowly as well. Perhaps a table of central wavelengths λ_j can be constructed for just a few surface skin temperature ranges with no adverse effect on the accuracy of the results obtained using Eq. (18) (for example, $\lambda_j = 11.87\mu m$ for 190-225 K; $11.84\mu m$ for 225-275 K; and $11.79\mu m$ for 275-330 K). As this report presents only potential methods for retrieving improved skin temperatures, the construction of a table of central wavelengths for the OLS-T and AVHRR thermal channels is deferred as one of several tasks of the RTNEPH attenuation study.

5. CANDIDATE INFRARED TRANSMITTANCE MODELS FOR WATER VAPOR LINE ABSORPTION

Having developed the theory necessary for determining attenuation corrections in the RTNEPH, the problem is reduced to computing atmospheric transmittances in real-time using a sensible, accurate, and efficient technique. Before proposing candidate models, it is helpful first to discuss what the difficulties are in computing reliable transmittances, especially under real-time operational constraints.

5.1 Narrow Band Transmittance Functions

Equation (4a) is for monochromatic radiation R_λ only. It must be convolved with the sensor response function $\phi_j(\lambda)$, as given by Eq. (4b), before it can be used to compute the radiance R_j measured in the spectral interval of a broadband LWIR instrument *j*. There is no analytic solution to Eqs. (4a) and (4b); they must be integrated numerically.

To integrate Eq. (4b) numerically requires that Eq. (4a) be evaluated for a large number of "closely spaced" values of wavelength λ that fall between λ_{j1} and λ_{j2}. If the separation $\Delta\lambda$ between wavelength values has to be very small before accurate radiances can be calculated, this procedure could be too cumbersome for real-time applications. If $\Delta\lambda$ is too large, then computed radiance errors result that are comparable to or larger than the noise in the satellite radiance measurements (Weinreb and Hill, 1980).

Consider dividing the thermal IR spectral band from λ_{j1} to λ_{j2} into subintervals, each of which is small enough so that the clear-column radiance R_n within the interval *n* is well approximated by

$$R_n = B_n(T_{sfc})\,\tau_{n,sfc} + \int_{p_{sfc}}^{0} B_n[T(p')]\frac{\partial \tau_n}{\partial p'}dp', \qquad (19a)$$

where the Planck radiance $B_n(T) = B(\lambda_n, T)$, λ_n is the central wavelength for subinterval *n*, and where

$$\tau_n = \bar{\tau}_{line}\,\bar{\tau}_{sb}\,\bar{\tau}_f. \qquad (19b)$$

The narrow band transmittance τ_n as given by Eq. (19b) is the average transmittance for the spectral subinterval *n* due to water vapor absorption. From Eq. (19b) it is easy to see that the narrow band water vapor transmittance can be treated in a simple analytic fashion as a product of the average spectral line and the continuum transmittances. $\bar{\tau}_{line}$ is the average transmittance due to water vapor line absorption; $\bar{\tau}_{sb}$ is due to collisions among water vapor molecules (called the self-broadened continuum); and $\bar{\tau}_f$ is due to collisions between water vapor molecules and other

constituent molecules along the path (called the foreign-broadened continuum). The average transmittance can be expressed as the product of $\bar{\tau}_{line}$, $\bar{\tau}_{sb}$, and $\bar{\tau}_f$ for intervals $\Delta\lambda_n = \lambda_{n2} - \lambda_{n1}$ that are small since the continuum transmittances are the components of the total transmittance that have a weak dependence on wavelength.

By dividing up a spectral band into several smaller subintervals, Eqs. (19a) and (19b) can be used to determine the radiance R_n within each subinterval n. Then to estimate the radiance R_j measured over the entire satellite sensor j bandwidth, compute a weighted sum

$$R_j = \frac{\sum_{n=1}^{N} R_n f_n}{\sum_{n=1}^{N} f_n}, \tag{19c}$$

where N is the number of subintervals in the domain from λ_{j1} to λ_{j2} ; and where the weights f_n are given by

$$f_n = \frac{\int_{\lambda_{n1}}^{\lambda_{n2}} \phi_j(\lambda)\, d\lambda}{\Delta\lambda_n},$$

which is the average of the response function ϕ_j within the subinterval from λ_{n1} to λ_{n2}. Equations (19a)-(19c) are approximations to Eqs. (4a) and (4b) that lend themselves more easily to computation. The accuracy of Eq. (19) is a function of the behavior of the Planck radiances $B(\lambda_n,T)$ and the transmittance $\tau(\lambda_n)$ as temperatures and wavelengths change. Weinreb and Hill (1980) have estimated that the errors incurred in using the approximations (19) are no worse than AVHRR sensor noise ranges. However, the effects of the assumptions that went into formulating Eq. (19) will be determined more carefully to ensure that no serious errors are incurred when computing satellite radiances R_j.

The monochromatic atmospheric transmittance $\tau_\lambda(p)$ at wavelength λ for the path between the top of the atmosphere and any pressure level p is given by

$$\tau_\lambda(p) = e^{-\delta_\lambda(p)}, \tag{20a}$$

where $\delta_\lambda(p)$ is the optical depth for the atmospheric path. For the LWIR region where water vapor is the primary absorber, optical depth is defined as

$$\delta_\lambda(p) = -\frac{1}{g}\int_{p}^{0} k_\lambda(p')\, q(p')\, dp', \tag{20b}$$

where g is the acceleration of gravity, k_λ is the cross-section absorption coefficient for water vapor (area per unit mass), and q is the specific humidity of water vapor (dimensionless). In general the absorption coefficient k_λ changes along an atmospheric path as a function $k_\lambda(p,T)$ of pressure and temperature along that path. The wavelength dependence of the absorption coefficient is significant as well.

The average line transmittance $\bar{\tau}_{line}$ [see Eq. (19b)] in the narrow band $\lambda_{n1} \leq \lambda \leq \lambda_{n2}$ for the path between the top of the atmosphere and any pressure level p is

$$\bar{\tau}_{line} = \frac{1}{\Delta\lambda} \int_{\lambda_{n1}}^{\lambda_{n2}} \tau_\lambda \, d\lambda, \tag{20c}$$

where τ_λ is the monochromatic transmittance due to water vapor line absorption. Substituting Eqs. (20a) and (20b) into Eq. (20c) yields the narrow band transmittance for the inhomogeneous path between the top of the atmosphere and any pressure level p:

$$\bar{\tau}_{line}(p) = \frac{1}{\Delta\lambda} \int_{\lambda_{n1}}^{\lambda_{n2}} \exp\left[-\frac{1}{g} \int_{p}^{0} k_\lambda(p') \, q(p') \, dp' \right] d\lambda \, . \tag{21}$$

where λ_{n1} and λ_{n2} are the endpoints of subinterval n, and $\Delta\lambda_n = \lambda_{n2} - \lambda_{n1}$. Equation (21) represents the only mathematically rigorous way of treating the dependence of transmittance on pressure, temperature, and wavelength. However it is difficult to evaluate the pressure-dependent integral in Eq. (21) separately for each wavelength inside the spectral subinterval $[\lambda_{n1},\lambda_{n2}]$ because of the complex dependence of absorption coefficient on temperature, pressure, and wavelength.

5.1.1 TRANSMITTANCE FUNCTION PARAMETERIZATIONS

There are band models available that approximate the atmospheric profiles of $\bar{\tau}_{line}(p)$ for an inhomogeneous path using transmittance models for homogeneous paths along which temperature and pressure are constant. Such models are easier to develop because the complicated (p,T) dependence of the average transmittance integral in Eq. (21) is simplified.

Consider a homogeneous atmospheric path along which pressure p and temperature T are constants p_0 and T_0 , respectively. The monochromatic optical depth δ_λ for a wavelength in the LWIR water vapor absorption region is simply [from Eq. (20b)]

$$\delta_\lambda(u) = k_\lambda u,$$

where the absorption coefficient k_λ is a function $k_\lambda\,(p_0,T_0)$ of wavelength and the constant path pressure and temperature, and where

$$u = \int_{s_1}^{s_2} \rho(s')ds'$$

is the water vapor absorber amount along the layer path ds′ from s_1 to s_2. Then the average band transmittance $\bar{\tau}$ for the homogeneous layer [from Eq. (21)] is precisely

$$\bar{\tau}_{line}\,(p_0,T_0,u) = \frac{1}{\Delta\lambda}\int_{\lambda_{n1}}^{\lambda_{n2}} e^{-k_\lambda(p_0,T_0)u}\,d\lambda\,. \qquad (22)$$

The above integral has no closed form and must be evaluated numerically. The absorption coefficient is an extremely complicated, strongly varying function of wavelength. To evaluate Eq. (22) accurately requires that the absorption coefficient k_λ be computed at many wavelengths between λ_{n1} and λ_{n2} so that it is computationally prohibitive to perform in a real-time or routine sense.

Equations (19a) and (19c) are simple to compute; the biggest problem lies in computing the average transmittances τ_n as given by Eq. (19b), and in particular the average line transmittance $\bar{\tau}_{line}$ as given by Eq. (22). As it stands, Eq. (22) is no easier to evaluate than Eq. (4b); a computationally prohibitive integration over some bandwidth is required by both equations if accurate results are to be obtained. The only difference between the two is that in Eq. (22), monochromatic transmittances $e^{-k_\lambda u}$ are averaged, while in Eq. (4b) radiances R_λ are averaged.

There are models available for computing reliable transmittances, but they are too slow to be considered for use by real-time applications such as the RTNEPH. One such example is the FASCODE model developed at the Geophysics Laboratory. FASCODE is a radiative transfer program that computes monochromatic transmittances as given by Eq. (21) (for more FASCODE information, see Clough et al, 1981). Its mathematically accurate treatment of absorption is obtained at the expense of routines that are so computationally intensive they cannot be used in real-time. However, FASCODE can be used to develop, test, and verify transmittance models for the RTNEPH that perform quickly, but still compute transmittances to a level of accuracy sufficient for the proposed cloud analysis radiance techniques to work successfully. Two such models are discussed in the following paragraphs.

Multivariate Polynomial Regression. The water vapor line transmittances $\bar{\tau}_{line}$ can be computed using a method that requires less time and memory than does a line-by-line technique such as FASCODE, but is nearly as accurate (Weinreb and Hill, 1980). The method follows that of Weinreb and Neuendorffer (1973), and is a least-

squares regression fit of the following 14-parameter polynomial to transmittances that were calculated using a full-scale, line-by-line model. For a homogeneous layer in which temperature and pressure are constant, the transmittance can be expressed by

$$\ln\left(-\ln \bar{\tau}_{\text{line}}\right) = \sum_{i=1}^{14} C_i(\lambda_n)\, X_i\,, \tag{23a}$$

where $\bar{\tau}_{\text{line}}$ is the water vapor line transmittance averaged over subinterval n, and where

$$\begin{aligned}
&X_1 = 1\,, && X_2 = 0.1 \ln\left[\, U \frac{T}{273} \,\right], && X_3 = \ln\left[\, \frac{p}{1000} \,\right],\\
&X_4 = \ln\left[\, \frac{T}{273} \,\right], && X_5 = X_2\, X_3\,, && X_6 = X_2\, X_4,\\
&X_7 = X_2{}^2\,, && X_8 = X_4\, X_7\,, && X_9 = X_3\, X_4,\\
&X_{10} = X_2\, X_7\,, && X_{11} = X_4\, X_6\,, && X_{12} = X_4{}^2,\\
&X_{13} = X_3\, X_6\,, && X_{14} = X_3\, X_7
\end{aligned} \tag{23b}$$

where p, T, and U are the constant pressure, constant temperature, and water vapor absorber amount, respectively, along a path in the homogeneous layer. The polynomial coefficients $C_i(\lambda_n)$ are derived from the least-squares regression over a large sample of pre-computed homogeneous path transmittances using a line-by-line method as specified by (22). Weinreb and Hill (1980) list a set of coefficients in their paper for the 3.5 - 4.1 and 10.2 - 12.9μm regions. These spectral intervals cover the DMSS OLS and NOAA AVHRR thermal channels.

Correlated k Distribution. In the following paragraphs the correlated k method is presented and its strengths and limitations discussed. The correlated k method retains many of the characteristics of an intensive line-by-line transmittance calculation, but it computes transmittances much more quickly and efficiently. Therefore, it is another candidate technique for real-time use by the RTNEPH.

The variable of integration in Eq. (22) is over the independent variable λ, with $k_\lambda(p_0,T_0)$ being the primary dependent variable. Rather than integrating over wavelength, Eq. (22) can be expressed as an integration over values of absorption coefficients whereby the transmissivity $e^{-k_\lambda u}$ is convoluted with the frequency of occurrence P(k) that absorption value k occurs within the spectral interval n, where $\lambda_{n1} \le \lambda \le \lambda_{n2}$. Rewritten in this form, the transmittance [Eq. (22)] becomes

$$\bar{\tau}_{\text{line}}\,(p_0,T_0,u) = \int_0^\infty P(k)\, e^{-ku}\, dk\,, \tag{24}$$

where P(k)dk is the frequency of occurrence of absorption coefficient between k and k+dk within the spectral subinterval n. Equation (24) expresses the band transmittance as a mean or "expected" value of transmissivity between λ_{n1} and λ_{n2}, where P(k) represents a normalized absorption coefficient density function for the band at some pressure p_0 and temperature T_0. If P(k) is known exactly, then (24) yields exactly the same result as Eq. (22).

The cumulative absorption coefficient distribution function g(k) is defined as

$$g(k) = \int_0^k P(k')\, dk' , \tag{25a}$$

so that g(k) is the fractional occurrence of absorption coefficient less than or equal to k. The value of g(k) must lie between 0 and 1. Differentiating Eq. (25a) yields

$$dg(k) = P(k')\, dk' . \tag{25b}$$

Noting that when k=0, g=0 and when $k = \infty$, $g = 1$, Eq. (24) can be rewritten with g as the variable of integration:

$$\bar{\tau}_{line}(p_0,T_0,u) = \int_0^1 e^{-k_g(p_0,T_0)u}\, dg , \tag{26}$$

where $k_g(p_0,T_0)$ is simply the inverse of the function g(k). If $k_g(p_0,T_0)$ is known exactly, then Eq. (26) yields exactly the same result as Eq. (22). Note that Eq. (26) differs from Eq. (22) only by the variable of integration; g has replaced λ.

The following example illustrates the steps that transform Eq. (22) into Eq. (26). Consider a simple spectral subinterval n with 10 equally-spaced wavelengths λ_1, λ_2, ... , λ_{10} that has the simple absorption coefficient spectrum plotted in Figure 2 (top). From Eq. (22), the average band transmittance $\bar{\tau}_{line}$ for this discrete case is

$$\bar{\tau}_{line}(p_0,T_0,u) = \frac{1}{10} \sum_{m=1}^{10} e^{-k_{\lambda_m}(p_0,T_0)u}\, \Delta\lambda_m .$$

Substituting the values plotted in Figure 2 (top) with $\Delta\lambda_m \equiv m+1 - m = 1$ yields

$$\bar{\tau}_{line} = \frac{1}{10} \left[e^{-k_1 u} + e^{-k_3 u} + e^{-k_4 u} + e^{-k_3 u} + e^{-k_1 u} + e^{-k_1 u} + e^{-k_3 u} + e^{-k_6 u} + e^{-k_3 u} + e^{-k_1 u} \right]$$

since $k_{\lambda_1}(p_0,T_0) = k_1$, $k_{\lambda_2}(p_0,T_0) = k_3$, ... , $k_{\lambda_{10}}(p_0,T_0) = k_1$. Combining like terms, the above equation can be rewritten as

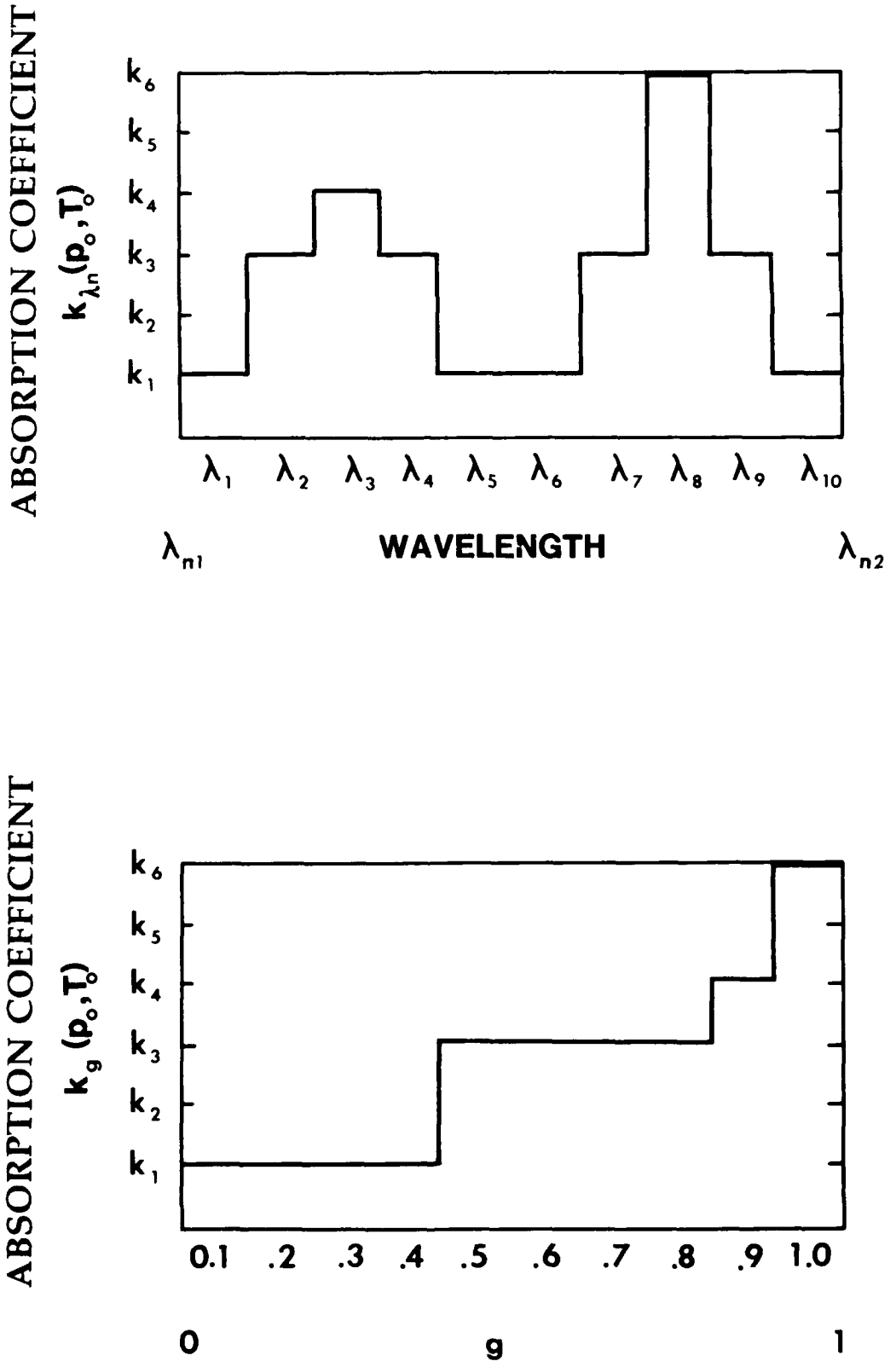

Figure 2. Plot of a Simple Absorption Spectrum in Wavelength Space (Top), and the Same Spectrum in "g" Space (Bottom)

$$\bar{\tau}_{line}(p_0,T_0,u) = \frac{1}{10}\left[4e^{-k_1 u} + 4e^{-k_3 u} + e^{-k_4 u} + e^{-k_6 u}\right]$$

$$= 0.4\, e^{-k_1 u} + 0.4\, e^{-k_3 u} + 0.1\, e^{-k_4 u} + 0.1\, e^{-k_6 u}. \qquad (27)$$

Next the average transmittance $\bar{\tau}$ will be evaluated using Eq. (26), and the result compared to Eq. (27). Before evaluating Eq. (26) for the Figure 2 case, the absorption spectrum first must be transformed from wavelength space to g space. The transformation that takes place between Eqs. (22) and (26) is illustrated by comparing the top and bottom plots of Figure 2. What occurs as a result of this transformation is that the absorption coefficients are shuffled from their original, random order in wavelength space into an orderly, monotonic arrangement in g space. The smallest values of g correspond to the smallest values of the absorption coefficient k, and the largest values of g correspond to the largest values of k.

In order to evaluate Eq. (26) for this example, note from Figure 2 (bottom) that $g_1 = 0.1$, $g_2 = 0.2$, ... , $g_{10} = 1$ and in general $g_m = 0.1m$. Therefore the average band transmittance $\bar{\tau}$ using Eq. (26) for the simple, discrete case under consideration is

$$\bar{\tau}_{line}(p_0,T_0,u) = \sum_{m=1}^{10} e^{-k_{g_m}(p_0,T_0)u}\,\Delta g_m .$$

Substituting in the absorption coefficient values for the spectrum plotted in Figure 2 (bottom) with $\Delta g_m = g_{m+1} - g_m = 0.1(m+1) - 0.1m = 0.1$ yields

$$\bar{\tau} = 0.1\left[e^{-k_1 u} + e^{-k_1 u} + e^{-k_1 u} + e^{-k_1 u} + e^{-k_3 u} + e^{-k_3 u} + e^{-k_3 u} + e^{-k_3 u} + e^{-k_4 u} + e^{-k_6 u}\right]$$

since $k_{g_1}(p_0,T_0) = k_1$, $k_{g_2}(p_0,T_0) = k_1$, ... , $k_{g_{10}}(p_0,T_0) = k_6$. Associating like terms, the above equation can be rewritten as

$$\bar{\tau}_{line}(p_0,T_0,u) = 0.1\left[4e^{-k_1 u} + 4e^{-k_3 u} + e^{-k_4 u} + e^{-k_6 u}\right]$$

$$= 0.4\, e^{-k_1 u} + 0.4\, e^{-k_3 u} + 0.1\, e^{-k_4 u} + 0.1\, e^{-k_6 u}, \qquad (28)$$

which is precisely the transmittance value given by Eq. (27). This simple example illustrates that the two forms [Eqs. (22) and (26)] for the transmittance $\bar{\tau}$ are identical.

The advantage of transforming the absorption spectrum from wavelength space to g space lies in the simplicity of evaluating the average band transmittance integral.

In order to accurately evaluate Eq. (22) (in wavelength space), the absorption coefficient k_λ must be computed at thousands of values of λ within spectral subintervals $\lambda_{n1} \leq \lambda \leq \lambda_{n2}$ that are only 0.2-0.4 μm in width. This is because the absorption coefficient is a quickly varying function of wavelength, so that sampling it at relatively widely-spaced values of λ will miss the fine, detailed wavelength structure that is so critical to accurate calculations of average transmittance. On the other hand, Eq. (26) (in g space) yields an accurate transmittance based upon approximately ten values of g, because the inverse cumulative distribution function k(g) exhibits a smooth monotonic behavior that makes it far less sensitive to sampling errors than is $k(\lambda)$.

This point is illustrated reasonably well by comparing the plots of Figure 2. There is a more complex shape to the top plot of absorption coefficient versus wavelength, while the bottom plot of absorption coefficient versus g is smooth and well behaved. The point is even better illustrated by comparing the Figure 3 plots of a more physically plausible absorption spectrum and its associated inverse cumulative absorption distribution. Note how far less critical it is to sample the absorption spectrum in g space (bottom plot) as frequently as it is in wavelength space (top plot). The absorption spectrum structure will likely be missed if it is sampled at wavelength values that are too far apart from each other, because the function $k(\lambda)$ changes so quickly with small changes in wavelength. However, the inverse cumulative distribution function k(g) is smooth and changes monotonically with g, so that its structure will be captured far more effectively when it is sampled at relatively widely spaced values of g. Thus, because fewer points are needed to sample the absorption spectrum, evaluating the average transmittance integral Eq. (26) is computationally much faster than having to evaluate Eq. (22), while still retaining a high accuracy.

5.1.2 APPLICATION TO INHOMOGENEOUS PATHS

To this point the transmittance models discussed have only applied to homogeneous paths. In this section, the theory will be presented for applying these models to inhomogeneous paths, that is, to paths along which temperature, pressure, and water vapor absorber amounts change.

Multivariate Polynomial Regression. The Weinreb technique is readily adaptable to computing transmittances in the thermal OLS band. The technique lends itself to real-time, operational RTNEPH applications and is capable of meeting all RTNEPH water vapor attenuation requirements [as specified by Eqs. (19a)-(19c)] for accuracy and efficiency. The following subsection contains additional details on how the Weinreb approximation is applied to inhomogeneous atmospheres. However, interested readers are strongly advised to refer to details of the Weinreb technique in papers by Weinreb and Neuendorffer (1973) and Weinreb and Hill (1980).

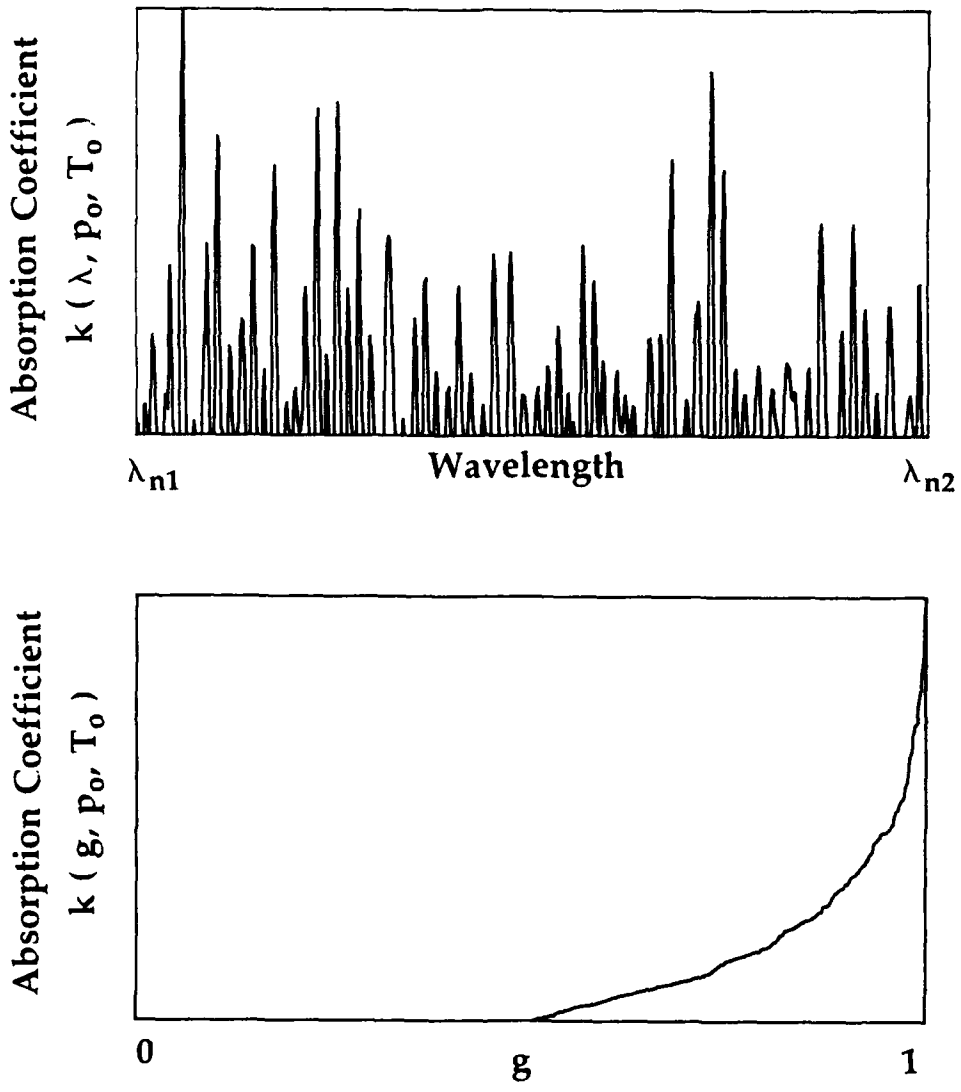

Figure 3. A More Physically Plausible Plot of Absorption Spectrum $k(\lambda)$ (Top) and Its Inverse Cumulative Absorption Distribution $k(g)$ (Bottom)

From Eq. (23b) it is easy to see that the transmittance $\bar{\tau}_{\text{line}}$ is a function $\bar{\tau}_{\text{line}}(p,T,U)$ of the pressure, temperature, and water vapor amount in some homogeneous layer. This is of little practical value for atmospheric paths that are inhomogeneous, that is, along which pressure, temperature, and mixing ratios change significantly between the top of the atmosphere and the ground. Consider dividing up such a path into a sequence of homogeneous layers each of which has p, T, and U constant. If the transmittances $\bar{\tau}_{\text{line}}$ were not a band average but rather truly monochromatic for some wavelength λ, then the total atmospheric transmittance over the inhomogeneous path from the surface to the top of the atmosphere would be the product

$$\tau_{\text{line}}(\lambda) = \prod_{l=1}^{L} \tau_{\text{line}}(p_l, T_l, U_l, \lambda) ,$$

where $\tau_{\text{line}}(\lambda)$ is the monochromatic transmittance due to water vapor line absorption, and where p_l, T_l, and U_l are the homogeneous pressure, temperature, and water vapor amount, respectively, for layer l; and where L is the number of layers into which the atmosphere has been subdivided.

If Eq. (23) were used to compute the layer transmittances $\tau_{\text{line}}(p_l,T_l,U_l,\lambda)$ on the right side of the above equation, the total atmospheric attenuation $\tau_{\text{line}}(\lambda)$ would be miscalculated. This is because the transmittance along the inhomogeneous path is simultaneously dependent on all the conditions (p_1,T_1,U_1), (p_2,T_2,U_2), ... , (p_L,T_L,U_L). The technique that is used for inhomogeneous paths is as follows.

Equation (23) establishes a relation

$$\bar{\tau}_{\text{line}} = \bar{\tau}_{\text{line}}(p, T, U) \tag{29a}$$

between transmittance and pressure, temperature, and water vapor amount. There is also a relation

$$U = U(\bar{\tau}_{\text{line}}, p, T) \tag{29b}$$

that equates average transmittance $\bar{\tau}_{\text{line}}$ to water vapor amount U for a given p and T. The relation (29b) is determined simply by solving Eq. (23) for U. With these functional relationships established, the Weinreb approximation to inhomogeneous paths can be described.

Consider an atmosphere composed of L homogeneous layers each of some pressure, temperature, and absorber amount p_l, T_l, and U_l, respectively. The total transmittance from the top of the atmosphere through the first layer (the top layer) is simply

$$\bar{\tau}_{\text{line}}(p_1, T_1, U_1), \tag{30a}$$

which for notational simplicity shall be called τ_1. For the transmittance τ_2 through both the first and the second layers, there is a bit of a dilemma. Equation (23) only computes transmittances for single values for p, T, and U; what is needed now is the transmittance for a path along which p, T, and U change.

The total amount of water vapor in the path through layers 1 and 2 is given by the sum $U_1 + U_2$. If the pressure and temperature through layers 1 and 2 are approximated by p_2 and T_2, then the total transmittance τ_2 for the path through the first two layers generally will be underestimated if it is computed as

$$\tau_2 \;=\; \bar{\tau}_{\text{line}}(p_2, T_2, U_1+U_2). \tag{30b}$$

However, there is a value

$$U_2^* \;=\; U_2 + \Delta U_2$$

with which the total transmittance τ_2 under both conditions p_1, T_1, and p_2,T_2 can be well approximated as a function $\tau_2 = \bar{\tau}_{\text{line}}(p_2, T_2, U_2^*)$. U_2^* is called the scaled water vapor amount, and is the sum of the known amount of water vapor U_2 in layer 2 and the unknown ΔU_2 whose value must be determined. For the path between the top of the atmosphere and the bottom of layer 2,

$$\tau_2 \;=\; \bar{\tau}_{\text{line}}(p_2, T_2, U_2+\Delta U_2).$$

But at the boundary between layer 1 and layer 2 the total atmospheric transmittance is τ_1. Also, at the very top of layer 2, the water vapor amount U_2 is zero, so that the above equation is simply

$$\tau_1 \;=\; \bar{\tau}_{\text{line}}(p_2, T_2, \Delta U_2). \tag{31a}$$

The transmittance τ_1 is given by Eq. (30a); thus the only unknown in the above relation is the value ΔU_2. Using Eq. (29b) it is simply

$$\Delta U_2 \;=\; U (\tau_1, p_2, T_2), \tag{31b}$$

which states that ΔU_2 is precisely the amount of water vapor that specifies the transmittance τ_1 through the *first* layer, except under the conditions p_2, T_2 of the *second* layer. Again, the scaled absorber amount U_2^* is the sum $U_2 + \Delta U_2$ of the water vapor amount in layer 2 and the scaled amount for layer 2. Finally, the total transmittance τ_2 through layers 1 and 2 is given by

$$\tau_2 = \bar{\tau}_{\text{line}}(p_2, T_2, U_2+\Delta U_2). \tag{32}$$

In general $U_1 \geq \Delta U_2$, indicating that the total transmittance τ_2 between layers 1 and 2 is underestimated when using Eq. (30b) as opposed to Eq. (32).

For an atmosphere that has been subdivided into L homogeneous layers, a recurrence relation can be set up whereby

$$\begin{aligned} \tau_l &= \bar{\tau}_{\text{line}}(p_l, T_l, U_l + \Delta U_l), \quad \text{and} \\ \Delta U_l &= U(\tau_{l-1}, p_l, T_l) \qquad \text{for } l = 2, 3, ..., L, \end{aligned} \tag{33}$$

where $\tau_1 = \bar{\tau}_{\text{line}}(p_1 , T_1 , U_1)$ as given by Eq. (23). The above procedure is repeated L times to arrive at the average transmittance $\bar{\tau}_{\text{line}} = \tau_L$ in subinterval n, as required by Eq. (19b), where τ_L is the average transmittance due to water vapor line absorption for the inhomogeneous path between the top of the atmosphere and the ground.

Correlated k Distribution. Equation (26) can be accurately evaluated for a homogeneous path along which pressure and temperature are constant. However, pressure and temperature variations strongly influence the shape of absorption spectra and hence the associated cumulative absorption distribution. Thus k(g) is a function k(g,p,T) of pressure and temperature. In order to calculate transmittance for a path along which pressure and temperature are not constant, the following correlated absorption method is used.

Consider a spectral subinterval $[\lambda_{n1},\lambda_{n2}]$ within which the absorption lines are equally spaced and of equal intensity as shown in Figure 4. Consider also an atmosphere composed of L homogeneous layers within which pressure p_l and temperature T_l are constant. The difference between the absorption spectra from one layer to the next is due only to differences in layer pressure and temperature. For notational simplicity, let

$$k_l(g) = k (p_l, T_l, g)$$

for the l^{th} layer, where $l = 1, 2, ..., L$. (In this notation the subscript l denotes the pressure-temperature dependence of the absorption coefficient.)

For this idealized case, there is some wavelength λ which is associated with a value $k^{(1)}$ of the absorption coefficient in the first (topmost) layer, there is always the same set of precisely known values $k^{(2)}, k^{(3)}, ..., k^{(L)}$ of absorption coefficients in layers 2, 3, ..., L, respectively, that are associated with λ. Thus there is a one-to-one mapping and a complete correlation between the absorption coefficients (hence the name "correlated k") in the first layer and those in successively lower layers (see

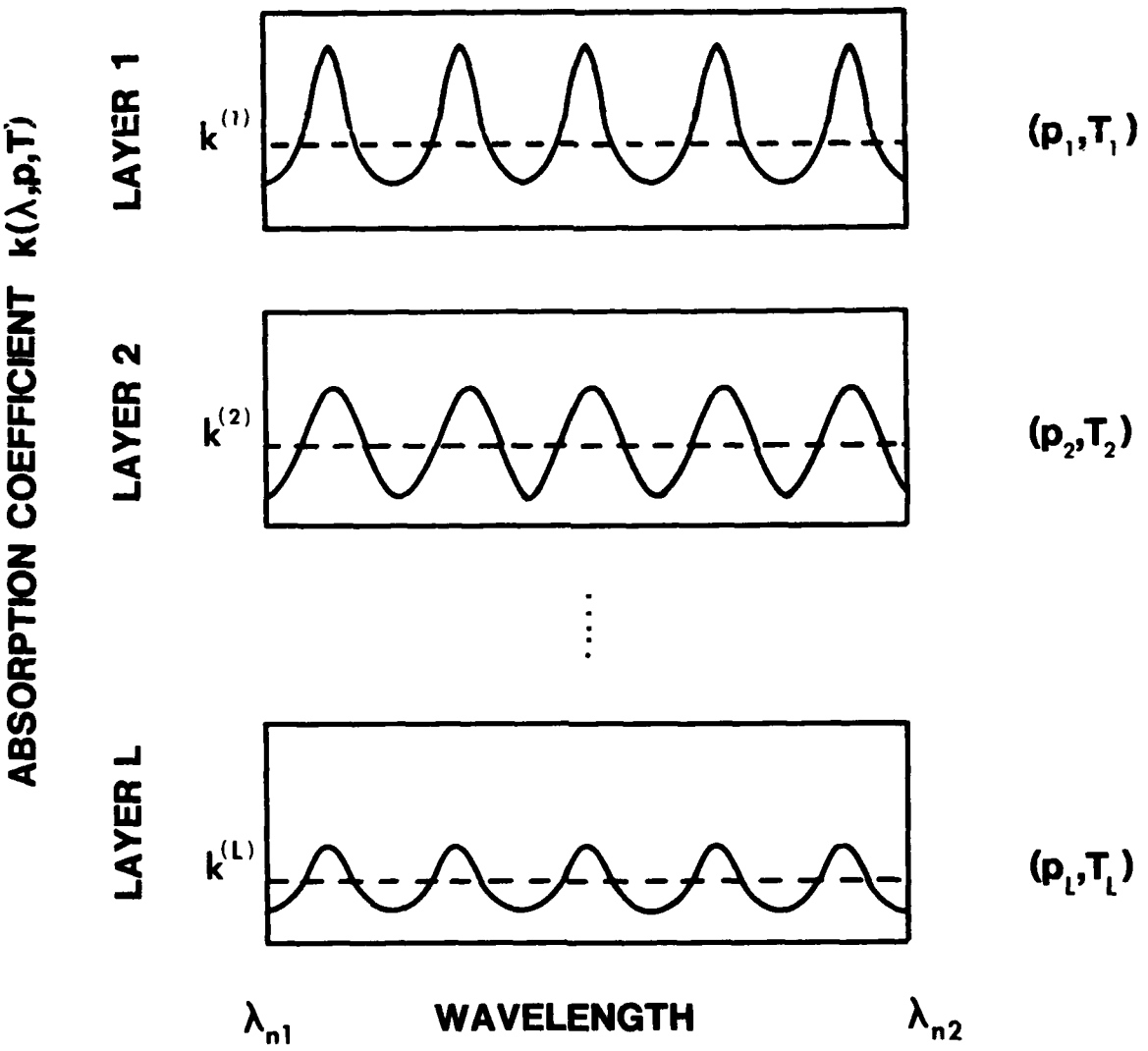

Figure 4. Plot of an Idealized Absorption Spectrum Profile Illustrating the Conditions Necessary for the Correlated k Transmittance Model to be Valid for an Inhomogeneous Atmospheric Path

Figure 4). It follows that the fraction of wavelengths with absorption coefficient values less than $k^{(1)}$ in layer 1 must be the same as the fraction of wavelengths with absorption coefficients less than $k^{(2)}, k^{(3)}, \ldots, k^{(L)}$ in layers 2, 3, ..., L, respectively. Mathematically, this is expressed as

$$g_1 (k^{(1)}) = g_2 (k^{(2)}) = \ldots = g_L (k^{(L)}) . \tag{34}$$

Simply stated, the percentile rank of absorption coefficient at a particular wavelength within a spectral subinterval remains unchanged from one layer to the next; that is, absorption coefficient rank is independent of pressure and temperature. For example, if absorption coefficient value $k^{(1)}$ is greater than 80 percent of the k values in layer 1, then $k^{(l)}$ is greater than 80 percent of the k values in layer l, for $l = 2, 3, \ldots, L$. Under these assumptions an inverse cumulative distribution function can be constructed for the optical depth of an inhomogeneous path of L layers by simply adding the optical depths for each homogeneous layer as a function of g; it is given by

$$\delta(g) = \sum_{l=1}^{L} k_l(g)\, u_l , \tag{35a}$$

where $k_l(g)$ is the inverse of the cumulative absorption coefficient distribution function $g_l(k)$ for layer l, and the absorber amount u_l for layer l is [from Eq. (20b)]

$$u_l = \frac{1}{g}\, q(p_l)\, \Delta p_l , \tag{35b}$$

where g is the acceleration due to gravity (the italic g denotes the acceleration constant as opposed to the correlated k transformation variable "g"), and where Δp_l is the thickness for layer l (in pressure units, positive-definite).

For this idealized case, then, the average transmittance $\bar{\tau}$ for the inhomogeneous path between the top of the atmosphere and some pressure level p_L is [from Eq. (26)]

$$\bar{\tau}_{\text{line}}(p_L) = \int_0^1 \exp \left[- \sum_{l=1}^{L} k_l(g)\, u_l \right] dg . \tag{35c}$$

Correlated k methods work best within absorption bands that satisfy the idealized conditions illustrated in Figure 4, and stated by Eq. (34). The extent to which Eq. (34) is valid dictates the accuracy of Eq. (35c). In other words, how well the absorption coefficients k(g) are correlated from one atmospheric layer to the next is the critical assumption that determines in general whether an accurate average transmittance value can be computed using a correlated k technique.

In the LWIR water vapor absorption spectrum, line strengths and spacings are

not uniform as they are for the idealized case in Figure 4. Temperature affects the strengths of some lines more strongly than others, especially for lines near the wings of molecular absorption bands. Hence, line strengths vary. In addition, the distance between lines is not even, causing lines to overlap in non-uniform ways as pressure and temperature change. For a value $k^{(1)}$ of absorption coefficient in layer 1 there exists not one but rather a range of values of absorption coefficients associated with $k^{(1)}$ in any subsequent layer. Because of these effects the absorption coefficients are not exactly correlated, as Eq. (34) specifies they should be.

However, the degree of lack of correlation is small; that is, the range of k values associated with $k^{(1)}$ is small so that Eq. (34) remains a good approximation. The high degree of correlation among absorption coefficients from one atmospheric layer to the next has allowed the correlated k method to be successfully applied to other problems.

From the previous subsection, recall that for a homogeneous layer the advantage of transforming the original absorption spectrum from wavelength space to g space lies in the simplicity of the spectrum shape (refer back to Figure 3). In g space the absorption spectrum k(g) is smoother and hence is less sensitive to discrete sampling errors than it is in wavelength space. By dividing up g space into several smaller subdomains, Eq. (35c) can be written in a quadrature form as

$$\bar{\tau}_{\text{line}}(p_L) = \sum_{i=0}^{I} \exp\left[-\sum_{l=1}^{L} k_l(g_i)\, u_l \right] \Delta g_i , \tag{36}$$

where I is the number of times the absorption spectrum $k_l(g_i)$ is to be sampled within the interval $0 \le g \le 1$. Equation (36) can be used to compute the average water vapor transmittance $\bar{\tau}_{\text{line}}$ [see Eq. (19b)] in the spectral subinterval $\lambda_{n1} \le \lambda \le \lambda_{n2}$ for the inhomogeneous atmospheric path between the top of the atmosphere and any pressure level p_L.

Techniques have been presented to compute narrow band water vapor line transmittances $\bar{\tau}_{\text{line}}$ [from Eq. (19b)] that are fast and accurate. The next section is devoted to presenting techniques that will be used to calculate the continuum transmittances τ_{sb} and τ_f [also from Eq. (19b)].

6. INFRARED TRANSMITTANCE MODELS FOR WATER VAPOR CONTINUUM ABSORPTION

Typically two types of water vapor continuum absorption are treated: self-broadened, which accounts for attenuation due to collisions between water vapor molecules, and foreign-broadened, which accounts for collisions among water vapor molecules and other atmospheric constituents. The self-broadened absorption is

dependent upon the partial pressure of water vapor, while foreign-broadened is dependent upon the partial pressure of the dry atmosphere (Weinreb and Hill, 1980).

6.1 Self-Broadened Continuum

The self-broadened average transmittance $\bar{\tau}_{sb}$ in spectral subinterval n for a path between the top of the atmosphere and some pressure level p is given by (Weinreb and Hill, 1980)

$$-\ln\left[\,\bar{\tau}_{sb}(p,\lambda_n)\,\right] \;=\; 5.41\times10^{13}\,C^{o}(\lambda_n)\,\sec\theta\int_{0}^{p} p'\,r^{2}\,e^{T_0\left(\frac{1}{T}-\frac{1}{296}\right)}\,dp', \qquad (37)$$

where p is the atmospheric pressure that specifies the end of the path; λ_n is the central wavelength for the spectral subinterval n from λ_{n1} to λ_{n2}; $C^{o}(\lambda_n)$ are coefficients determined for each subinterval n; θ is the angle between the atmospheric path and the local vertical (the zenith angle); r is the mass mixing ratio of water vapor (g/kg, dimensionless) at pressure level p'; T_0 is 1800 K for the $10.2-12.9\mu m$ region and 1300 K for the $3.5-4.1\mu m$ region; and T is the atmospheric temperature at pressure p'.

Equation (37) can be written in quadrature form for a sequence of L homogeneous layers in spectral subinterval n as

$$-\ln\left[\,\bar{\tau}_{sb}(p_L,\lambda_n)\,\right] \;=\; 5.41\times10^{13}\,C^{o}(\lambda_n)\,\sec\theta\sum_{l=1}^{L} p_l\,r_l^{2}\,e^{T_0\left(\frac{1}{T_l}-\frac{1}{296}\right)}\,\Delta p_l, \qquad (38)$$

where p_l, r_l, and T_l are the constant pressure, mixing ratio, and constant temperature, respectively, for homogeneous layer l; Δp_l is the thickness (in pressure coordinates) of layer l; and where all other variables are as in Eq. (37). The coefficients $C^{o}(\lambda_n)$ are listed in Weinreb and Hill (1980) for each subinterval n.

6.2 Foreign-Broadened Continuum

The foreign-broadened water vapor continuum average transmittance $\bar{\tau}_f$ in spectral subinterval n for a path between the top of the atmosphere and some pressure level p is given by (Weinreb and Hill, 1980)

$$-\ln\left[\,\bar{\tau}_{f}(p,\lambda_n)\,\right] \;=\; 4.04\times10^{15}\,C^{o}(\lambda_n)\,\sec\theta\int_{0}^{p} p'\,r\,dp', \qquad (39)$$

where p is the atmospheric pressure that specifies the end of the path; λ_n is the

central wavelength for the spectral subinterval n from λ_{n1} to λ_{n2} [the same as in Eq. (37)]; $C^o(\lambda_n)$ are coefficients determined for each subinterval n; θ is the angle between the atmospheric path and the local vertical (the zenith angle); and r is the mass mixing ratio of water vapor (g/kg, dimensionless) at pressure p'. In longwave thermal IR window regions, the foreign-broadened continuum absorption is negligible in comparison with self-broadened and line absorptions; thus Eq. (39) is ignored for 10.2 - 12.9μm.

Equation (39) can be written in quadrature form for a sequence of L homogeneous layers in spectral subinterval n as

$$-\ln [\, \bar{\tau}_f (p_L, \lambda_n) \,] \;=\; 4.04\times 10^{15}\, C^o(\lambda_n) \sec\theta \sum_{l=1}^{L} p_l\, r_l\, \Delta p_l , \tag{40}$$

where p_l, r_l, and T_l are the constant pressure, mixing ratio, and constant temperature, respectively, for homogeneous layer l; Δp_l is the thickness (in pressure coordinates) of layer l; and where all other variables are as in Eq. (39). Remember, Eq. (40) is for the 3.5 - 4.1μm spectral interval only; foreign-broadened continuum absorption *is ignored* in the 10.2 - 12.9μm region, but it cannot be ignored in the 3.5 - 4.1μm region (Weinreb and Hill, 1980).

Methods have been discussed that allow for quick, accurate computations of the average water vapor transmittance τ_n [as given by Eq. (19b)] over spectral subinterval n (from λ_{n1} to λ_{n2}) for an inhomogeneous atmospheric path. Using Eq. (19b), τ_n is well approximated as the product of the water vapor line transmittance $\bar{\tau}_{line}$ as given by either Eq. (33) (for the multivariate regression technique of Weinreb and Hill) or Eq. (36) (for the correlated k method), the self-broadened continuum transmittance $\bar{\tau}_{sb}$ as given by Eq. (38), and the foreign-broadened continuum transmittance $\bar{\tau}_f$ as given by Eq. (40).

7. OVERLAPPING ABSORPTION BANDS

The narrow band transmittance τ_n as given by (19b) is affected by absorption due to constituents other than water vapor, such as molecular nitrogen and the uniformly mixed gases. In formulating (19b) it was assumed that water vapor absorption is dominant in LWIR window regions. This is certainly the case for the OLS and AVHRR thermal IR channels; however, the absorption bands of molecular nitrogen and other uniformly mixed gases overlap the water vapor absorption bands within these channels and have small effects on total transmittance.

The transmittance τ_λ for a particular wavelength λ is affected by the quantity

and type of absorbers present in an atmospheric path. Assume for illustration that there are three types of absorbers *a, b,* and *c* in a path along which transmittance is to be computed. The total monochromatic transmittance along that path is given by

$$\tau_\lambda = \tau_a(\lambda)\,\tau_b(\lambda)\,\tau_c(\lambda),$$

where $\tau_a(\lambda)$ is the transmittance due to absorber type *a*, etc. Inserting this form into Eq. (20c) yields

$$\tau_n = \frac{\int_{\lambda_{n1}}^{\lambda_{n2}} \tau_a(\lambda)\,\tau_b(\lambda)\,\tau_c(\lambda)\,d\lambda}{\Delta\lambda_n}.$$

Thus the average total transmittance in spectral band *n* is the average of the products of the monochromatic transmittances for each absorber type along the path. If the spectral band is chosen to be small enough then the average total transmittance can be well approximated by

$$\tau_n \approx \frac{\int_{\lambda_{n1}}^{\lambda_{n2}} \tau_a(\lambda)\,d\lambda \int_{\lambda_{n1}}^{\lambda_{n2}} \tau_b(\lambda)\,d\lambda \int_{\lambda_{n1}}^{\lambda_{n2}} \tau_c(\lambda)\,d\lambda}{\Delta\lambda_n}.$$

In general the above equation is not precisely true except for monochromatic transmittances (that is, when $\lambda_{n1} = \lambda_{n2}$) or, for $\lambda_{n1} \neq \lambda_{n2}$, if the constituents *a, b,* and *c* have absorption characteristics that are completely uncorrelated with each other. However, the product of the average individual transmittances over the interval generally approximates well the average product of the monochromatic transmittances.

Thus, assuming that the spectral interval *n* is properly chosen, the average total transmittance τ_n as given by Eq. (19b) can be expressed as the product of the average transmittances for the individual absorbers. From the above equation, then, the average transmittance for spectral band *n* is

$$\tau_n \approx \bar{\tau}_{H_2O}\,\bar{\tau}_N\,\bar{\tau}_{gas}\ , \tag{41}$$

where

$$\bar{\tau}_{H_2O} = \bar{\tau}_{line}\,\bar{\tau}_{sb}\,\bar{\tau}_f$$

is the average transmittance for spectral band *n* due to water vapor line absorption

[see Eq. (19b)]; $\bar{\tau}_{sb}$ is due to collisions among water vapor molecules (the self-broadened continuum); $\bar{\tau}_f$ is due to collisions between water vapor molecules and other constituent molecules along the path (the foreign-broadened continuum); $\bar{\tau}_N$ is due to collision-induced molecular nitrogen absorption; and $\bar{\tau}_{gas}$ is the average band transmittance due to uniformly mixed gases (carbon dioxide, nitrous oxide, carbon monoxide, methane, and molecular oxygen).

There are techniques similar to Eqs. (38) and (40) that are available for use in computing $\bar{\tau}_N$ and $\bar{\tau}_{gas}$; examples are presented in Weinreb and Hill (1980). As previously mentioned, water vapor is the primary absorber for the thermal infrared wavelengths. As far as the RTNEPH is concerned, attenuation by molecular nitrogen is significant only in the region near 4.3μm, and the uniformly mixed gases absorb weakly in both the 3.7 and 10-12μm regions. Thus for RTNEPH purposes these effects will likely be neglected, since they are typically small in comparison to $\bar{\tau}_{H_2O}$.

8. DISCUSSION AND PLANS

Techniques have been presented that can be used to compute the expected IR water vapor attenuation along a given atmospheric path. Such computations are necessary for cloud/no-cloud threshold techniques (such as the RTNEPH IR processor) that compare a measured IR brightness temperature, which includes the effects of atmospheric water vapor attenuation, with a corresponding surface skin temperature. In this section, study plans are outlined to show how these attenuation models will be incorporated into the RTNEPH.

Before the homogeneous path transmittance model of Weinreb and Hill (see Section 5.1) can be incorporated into the RTNEPH, several minor efforts must first be completed. Recall from Eqs. (19a)-(19c) that the basic method for computing an expected clear-column IR radiance is initially to subdivide the thermal band of interest into smaller subintervals, compute an average radiance for each subinterval [Eqs. (19a) and (19b)], and then perform a weighted average of the subinterval radiances to get the total band radiance [Eq. (19c)]. The band radiance is then converted to an expected clear-column brightness temperature using Eq. (18). Currently the homogeneous path technique, originally developed for the relatively narrow AVHRR thermal channels, divides the broadband DMSS OLS-Thermal band into eight subintervals. A sensitivity study must be performed to ensure that these eight subintervals will allow for OLS-T radiance calculations of sufficient accuracy. (The complexity of the IR sensor response function along with the spectral variation of the Planck function across the band determines how many subintervals need to be chosen.) For purposes of comparison, errors in clear-column brightness temperature of less than 0.5 K from the line-by-line FASCODE brightness temperature will be the accuracy benchmark since 0.5 K will be roughly the thermal resolution of an 8-bit IR

SGDB.

The Weinreb and Hill continuum calculations [Eqs. (38) and (40)] will be replaced by the latest FASCODE water vapor continuum model. This task essentially involves updating the coefficients $C^{o}(\lambda_n)$ that appear in Eqs. (30) and (32), and formulating the (p,T) effects slightly differently (see Clough et al, 1981). Also, the water vapor line absorption regression coefficients $C_i(\lambda_n)$ in Eq. (23) may be recomputed (via multivariate regression to FASCODE water vapor line absorption transmittances) if it is determined that the line transmittances do not match those of FASCODE to within 1 or 2 percent. Such a tight constraint is necessary because small errors in transmittance can manifest themselves as larger errors in computed brightness temperature via the differential transmission term $\partial\tau_n / \partial p$ [see Eq. (19a)].

With these issues addressed, attention can then be focus on the implementation of a candidate transmittance model (either the multivariate polynomial regression or correlated k) into the RTNEPH operational framework. Validation runs will test the accuracy of the transmittance model against ground truth measurements of clear-column brightness temperature for a known atmospheric path. Among the data available for such tests include maritime radiosonde data in conjunction with a measured sea surface temperature and coincident IR brightness temperature measurements. (Such tests cannot be performed over land because of the unavailability of routine ground truth skin temperature measurements.) Other verification test data sources include coincident measurements of surface skin temperature, upper air temperature and water vapor profiles, and satellite-based IR radiance measurements obtained during the FIFE '89 summer land-surface/atmosphere field experiment over the Kansas plains.

Checks will also be performed against FASCODE runs to ensure the transmittance models are accurate. Initial comparisons have checked out to well within the 0.5 K tolerance, but several more FASCODE runs will be made over a range of globally-expected atmospheric paths, ranging from very dry at low viewing angles to very moist at high viewing angles. In terms of accuracy it is expected that the attenuation model will be more than adequate for the RTNEPH. It is more likely that any observed shortcomings in the transmittance calculations will be due to inaccurate and/or insufficient surface skin temperatures and atmospheric profile data available to the model.

Once the attenuation model is ready, the first step will be to compare its water vapor attenuation correction calculations to those currently performed by the RTNEPH. A study is now underway that computes the water vapor attenuation for upper air stations throughout North America over a period of several months. The chosen radiosonde stations are plotted in Figure 5. Note that a wide variety of tropical, maritime, arctic, and continental stations have been selected. The plan is to collect radiosonde data from these stations and run three LWIR water vapor

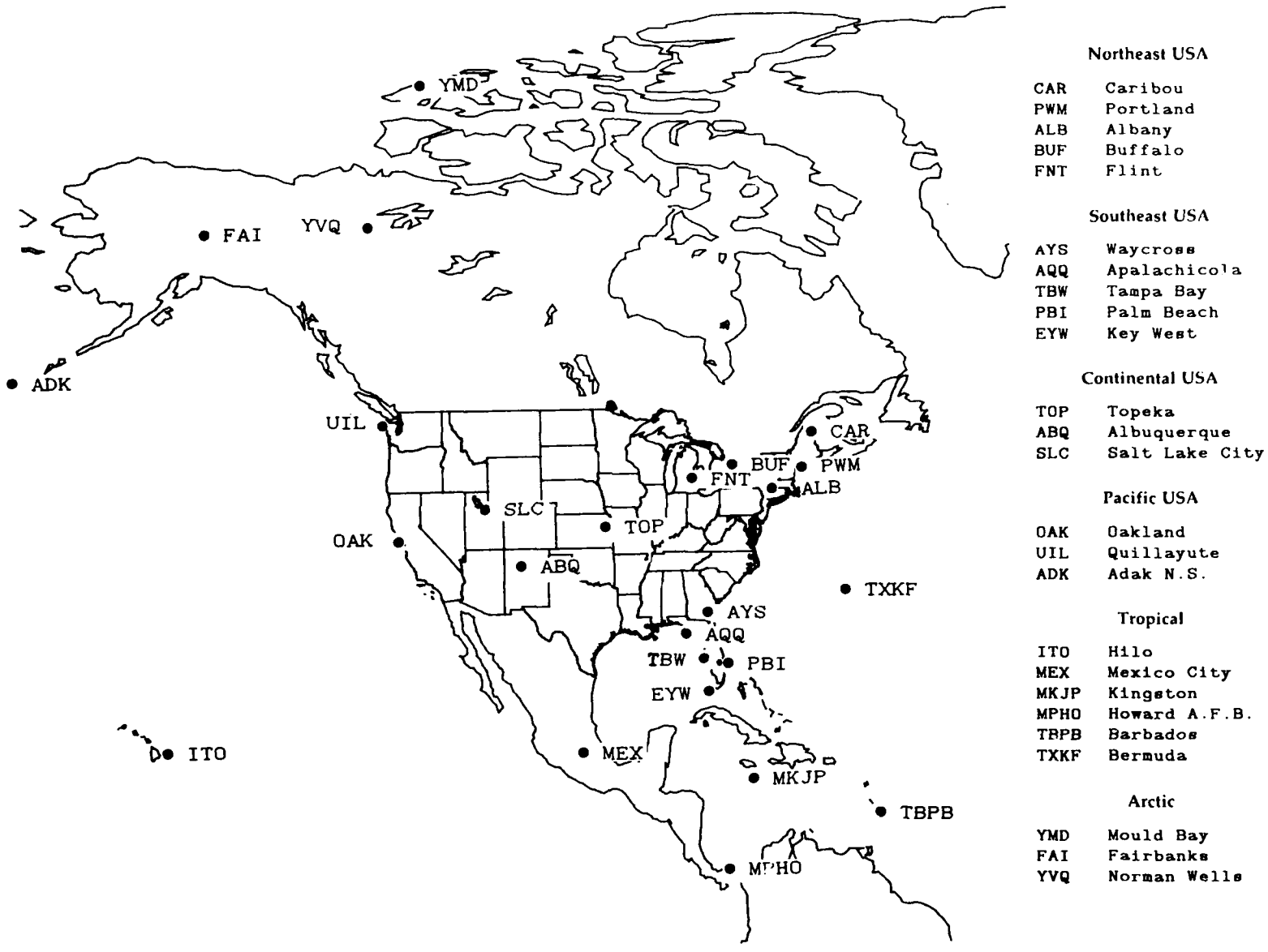

Figure 5. Radiosonde Stations Selected for the Water Vapor Attenuation Study

attenuation codes on their atmospheric profile data: the candidate RTNEPH technique (multivariate polynomial regression or correlated k), LOWTRAN (a parameterized version of FASCODE), and the current operational RTNEPH "lookup table" scheme. The current and proposed RTNEPH attenuation correction techniques will then be directly compared. Through this study the following issues will be directly addressed:

1. From a computational point of view, how complex does the transmittance model need to be in order to achieve a computed equivalent radiance error less than 0.5 K? Is the current RTNEPH attenuation scheme accurate enough or is a more sophisticated scheme warranted?

2. Is there an observed and significant fine-scale horizontal variation in water vapor attenuation that is captured by the resolution of the data in this study but that cannot be captured by the RTNEPH HIRAS upper air database? If this is so, does the whole-mesh upper air temperature profile somehow need to be updated throughout the boundary layer at eighth-mesh resolution using the local surface skin temperature measurement?

3. Is there a significant loss of information if significant level data are left out of the RTNEPH upper air temperature profiles (that is, if only mandatory level data are used)?

A preliminary estimate can likely be made through this study of how the proposed transmittance computations might affect the RTNEPH IR processor cloud/no-cloud analysis.

Currently, the RTNEPH uses four lookup tables to help determine water vapor attenuation corrections as a function of 1) IR grayshade, 2) sensor viewing angle, 3) whether the point of interest lies within the tropics, and 4) day/night, sea/land, and geographic location (that is, RTNEPH box). These complicated corrections are necessary because of biases in the spectral response for a particular IR sensor as it ages onboard a spacecraft, data truncation and viewing angle correction procedures that the IR SGDB software invokes on the raw satellite data before it is processed by the RTNEPH, and because OLS-Thermal data are not precisely calibrated. The attenuation correction techniques proposed in this paper will eliminate the need for the first three RTNEPH lookup table correction factors, replacing them with a physically rigorous and robust technique.

In and of itself, it is unrealistic to expect that the insertion of a physically sensible method of computing water vapor attenuation correction factors will eliminate all of

the errors in the RTNEPH cloud/no-cloud analysis. The attenuation computations may very well be accurate for the atmospheric profile data that were used to compute them. However, if these atmospheric data are themselves inaccurate, errors in the cloud analysis will likely occur. A need for including some type of bias correction will still exist even with the new attenuation model. Thus some type of lookup table that is a function of day/night, sea/land, and geographic location will likely be retained because of biases in the input data and uncertainties in sensor degradation effects.

The surface radiance term [first term on the right side of Eq. (19a)] is dominant in most IR upwelling radiance calculations. The surface radiance is strongly dependent on the surface skin temperature. Therefore, accurate values of surface skin temperature are important in computing clear-column radiances. To this end, improvements are being proposed and developed for the surface skin temperature model used by the RTNEPH IR processor threshold technique. Presumably the characteristics of the new skin temperatures will prompt a significant and nontrivial retuning effort of the current RTNEPH water vapor attenuation correction factors. At the same time GL is planning to develop and implement a new method for calculating these correction factors. If one upgrade (for either temperature or attenuation) becomes available and is implemented before the other, then a two-step process is envisioned whereby two long-term retuning periods will result; one after implementation of the new surface skin temperature model and another after implementation of the new attenuation correction model (or vice versa). It is therefore suggested that both enhancements be implemented into the RTNEPH coincidentally so as to minimize the length and complexity of the readjustment periods that the RTNEPH will undergo.

At first glance the attenuation correction computations outlined in this study may appear too complex and time-consuming for practical RTNEPH use. However, these models are fast, efficient, and very accurate. The most intensive transmittance computations will be performed on a whole mesh grid basis. For example, to compute an OLS-Thermal band transmittance profile and subsequent clear-column band radiance for a 15-layer atmosphere takes FASCODE 114 seconds of CPU time on a 3 MIPS MicroVAX 3600 computer; it takes the multivariate polynomial regression transmittance model 0.1 CPU seconds, faster by a factor of 1000.

A final determination will be made on the accuracy of the RTNEPH cloud/no-cloud decisions using the current and the proposed attenuation correction procedures. Comparisons of cloud fields derived using each procedure will be made directly against interactively-derived cloud truth fields [see Gustafson and Felde (1988) for a description of how RTNEPH cloud truth fields are generated]. Using these fields, biases inherent in the proposed attenuation correction procedures can be discovered and addressed. It is believed that an improved attenuation correction model will significantly increase the quality of the RTNEPH IR processor clear/cloud analysis. The manually intensive process of updating four RTNEPH attenuation correction

and bias lookup tables will be reduced to at most one bias table, with the other three tables being replaced explicitly by the techniques proposed in this paper. The proposed attenuation correction techniques can be easily transitioned to new sensors by simply changing the appropriate sensor response function values f_n in Eq. (19c). In the same way, data from the thermal AVHRR channels at 3.7, 10.7, and 11.8μm can be incorporated easily into the RTNEPH IR processor with a minimal recoding effort.

References

Bunting, James T., R. S. Hawkins, R. P. d'Entremont, and G. B. Gustafson, 1983: R&D nephanalysis at the Air Force Geophysics Laboratory. *Proc. Fifth Conf. on Atmospheric Radiation,* Amer. Meteor. Soc., 272-275.

Clough, S. A., F. X. Kneizys, L. S. Rothman and W. O. Gallery, 1981: Atmospheric spectral transmittance and radiance FASCODE 1B. *Proc. SPIE,* **277**, Atm. Transm.

Crum, Timothy D. (ed.), 1987: *AFGWC Cloud Forecast Models.* Air Force Global Weather Central Technical Memorandum AFGWC-TN-87-001, Offutt AFB, NE 68113, 73 pp.

d'Entremont, Robert P., R. S. Hawkins, and J. T. Bunting, 1982: *Evaluation of Automated Imagery Analysis Algorithms for Use in the Three-Dimensional Nephanalysis Model at AFGWC.* Air Force Geophysics Laboratory Technical Report AFGL-TR-82-0397, Hanscom AFB, MA 01731-5000, 39 pp., ADA131986.

d'Entremont, Robert P., G. B. Gustafson, J. T. Bunting, M. K. Griffin, C. Barker Schaaf, P. L. Nowak, J. M. Ward, and R. S. Hawkins, 1989: *Comparisons Between the RTNEPH and AFGL Cloud Layer Analysis Algorithms.* Air Force Geophysics Laboratory Technical Report AFGL-TR-89-0175, Hanscom AFB, MA 01731-5000, 63 pp. **ADA216637**

Fye, Falko K., 1978: *The AFGWC Automated Cloud Analysis Model.* Air Force Global Weather Central Technical Memorandum AFGWC-TN-78-002, Offutt AFB, NE 68113, 97 pp.

Gustafson, Gary B. and Gerald W. Felde, 1988: Interactive satellite image processing applied to cloud detection. Preprints, Fourth International Conference on Interactive Information and Processing Systems for Meteorology, Oceanography, and Hydrology, *Amer. Meteor. Soc.*, Boston MA, 100-103.

Kiess, Raymond B. and William M. Cox, 1988: *The AFGWC Automated Real-Time Cloud Analysis Model.* Air Force Global Weather Central Technical Memorandum AFGWC-TN-88-001, Offutt AFB, NE 68113, 82 pp.

Weinreb, Michael P. and Arthur C. Neuendorffer, 1973: Method to Apply Homogeneous-path Transmittance Models to Inhomogeneous Atmospheres. *Journ. Atmos. Sci.*, Amer. Meteor. Soc., **30**, 662-666.

Weinreb, Michael P. and Michael L. Hill, 1980: *Calculation of Atmospheric Radiances and Brightness Temperatures in Infrared Window Channels of Satellite Radiometers,* NOAA Technical Report NESS 80, U. S. Dept. of Commerce, Washington, D.C., 40 pp.